J Electroceram (2008) 21:353–356
DOI 10.1007/s10832-007-9155-x

Magnetic properties and thermal behavior of mullite–iron nanocomposite powders

Hao Wang · Wei-Min Wang · Zheng-Yi Fu · Tohru Sekino · Koichi Niihara

Published online: 1 May 2007

Abstract Mullite based iron magnetic nanocomposite powders were synthesized by reduction of sol–gel prepared mullite–iron oxide solid solution in hydrogen flow. Structural characterization studied by TEM revealed that two types of α-iron nanoparticles existed in mullite matrix. The α-iron nanoparticles with the size around hundreds of nanometers appeared as inter-type grains, while those around 10 nm were embedded in the grains of mullite. The magnetic properties of nanocomposites suggest that the intergranular and intragranular α-iron nanoparticles had the ferromagnetic and superparamagnetic behavior at room temperature, respectively. The oxidation behavior of nanocomposite powders showed that there existed two different oxidation stages of α-Fe nanoparticles.

Keywords Mullite · Iron · Nanocomposite · Magnetic properties · Oxidation behavior

1 Introduction

Iron based magnetic nanoparticles have been widely studied for applications on magnetic recording, magnetic fluids, magnetic resonance imaging contrast agents and environmental remediation [1–3]. Generally, iron nanoparticles are prepared from soluble precursors with some methods, such as thermal decomposition, sonochemical decomposition, electrochemical reduction or chemical reduction [4–7]. By thermal or sonochemical decomposition of iron pentacarbonyl in the presence of organic surfactants/dispersants (such as oleic acid or polymers), inorganic–organic nanocomposites with the dispersion of iron nanoparticles were synthesized. Moreover, the dispersion of iron nanoparticles in amorphous glass was also obtained by chemical reduction of iron oxides contained silica. Actually, ceramic grains can also be used as effective dispersants for preparation of metal nanoparticles by chemical reduction of ceramic solid solutions [8]. Since metal nanoparticles nucleate and grow inside ceramic grains, the particle growth is restricted. It becomes possible to prepare intragranular nanocomposite with metal nanoparticles embedded in ceramic grains.

As the only stable crystalline phase formed at atmospheric pressure in the aluminosilicate (Al_2O_3–SiO_2) system, mullite is widely researched. Due to its superior thermal and physicochemical properties, such as low thermal expansion, good thermal shock resistance, high melting point, high chemical stability, and infrared transparency, mullite has been considered as an important material for high-temperature structural, electronical, and optical applications [9]. Besides the replacement of Si^{4+} and Al^{3+} that leads to the formation of non-stoichiometric compound, mullite can also incorporate different amounts of transition metal cations by substitution of Al^{3+} ion at different positions [10]. In the case of Fe-doped mullite, 12 wt% Fe_2O_3 can be dissolved in mullite matrix under 1,200 °C by replacing the Al^{3+} at octahedral site [11]. In this paper, mullite–iron magnetic nanocomposite powders were prepared by reduction of sol–gel prepared mullite–iron oxide solid solution with a nominal composition of

H. Wang (✉) · W.-M. Wang · Z.-Y. Fu
State Key Lab of Advanced Technology for Materials Synthesis and Processing, Wuhan University of Technology, Wuhan 430070, People's Republic of China
e-mail: shswangh@mail.whut.edu.cn

T. Sekino · K. Niihara
Institute of Scientific and Industrial Research (ISIR), Osaka University, Mihogaoka 8-1, Ibaraki, Osaka 567-0047, Japan

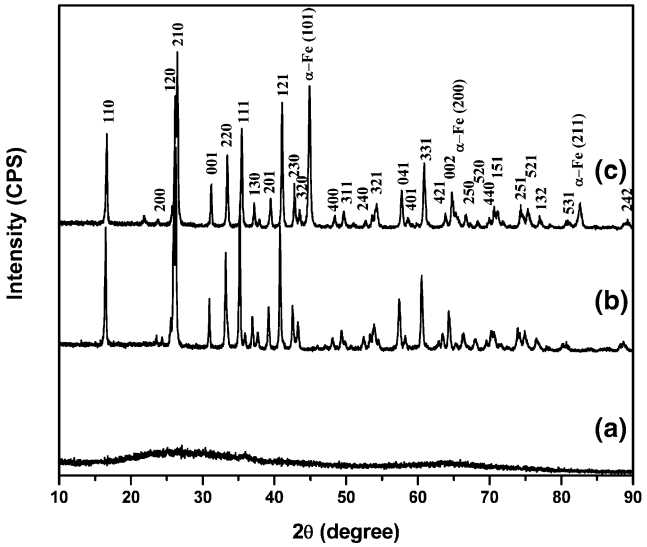

Fig. 1 XRD profiles of powders heat-treated at various temperatures and atmosphere. ((**a**) 500 °C, 2 h, air; (**b**) 1,200 °C, 4 h, air; (**c**) 1,300 °C, 1 h, H_2)

$Al_{5.4}Fe_{0.6}Si_2O_{13}$ in hydrogen flow at 1,300 °C. The microstructure, magnetic properties and oxidation behavior of nanocomposite powders were investigated.

2 Experimental procedures

The mullite–iron oxide solid solution with nominal composition of $Al_{5.4}Fe_{0.6}Si_2O_{13}$ was synthesized by heating the sol–gel made powders following the method described elsewhere [12]. $Al(NO_3)_3{\cdot}9H_2O$, $Fe(NO_3)_3{\cdot}9H_2O$ and Si $(OC_2H_5)_4$ were used as the precursors for alumina, iron oxide and silica, respectively. Dried gel powders were treated at 500 °C for 2 h in air to remove volatile substance and were successively calcinated at 1,200 °C for 4 h to form solid solution. To obtain the iron dispersed mullite nanocomposite powders, solid solution powders were reduced in flowing hydrogen gas at 1,300 °C for 1 h. The crystalline phases of samples were recorded by Rigaku RU-200B X-ray diffractometer with 50 KV and 200 mA using Cu Kα radiation. The microstructure of nanocomposite powders was observed by transmission electron microscope, Hitachi H-8100T. Measurement of magnetic properties was conducted on Quantum Design MPMS superconducting quantum interference device (SQUID) magnetometer. Zero-field-cooled and field-cooled magnetizations were determined with an applied field of 100 Oe between 10 K and 300 K. Oxidation behavior of nanocomposite powders was monitored by thermogravimetric and differential thermal analysis (TG-DTA; TG-DTA 2020SAF) in air at a heating rate of 10 °C/min from room temperature to 1,400 °C.

3 Results and discussion

XRD patterns of heat-treated powders at 500 °C, 1,200 °C, along with those powders reduced at 1,300 °C, are shown in Fig. 1. Powders remain amorphous after treated at 500 °C while volatile impurities have been completely eliminated. Through crystallization and reaction of oxide precursors, the mullite–iron oxide solid solution is the only phase detected by XRD after soaking at 1,200 °C. After reduction at 1,300 °C, the peaks of α-Fe appear in composite powders. It should be noted that the formation temperature is much higher than that of iron nanoparticles embedded in silica (around 500 °C [13]). Since Fe^{3+} locates in the lattice of mullite, high temperature is essential to supply enough reduction and diffusion ability to hydrogen. The TEM images of reduced powders are shown in Fig. 2. Two kinds of α-Fe nanoparticles with different particle sizes were observed. Some α-Fe grains with sizes larger than 200 nm are formed by the aggregation and growth of the iron nanoparticles located on or near the surface of the solid solution grains. Other

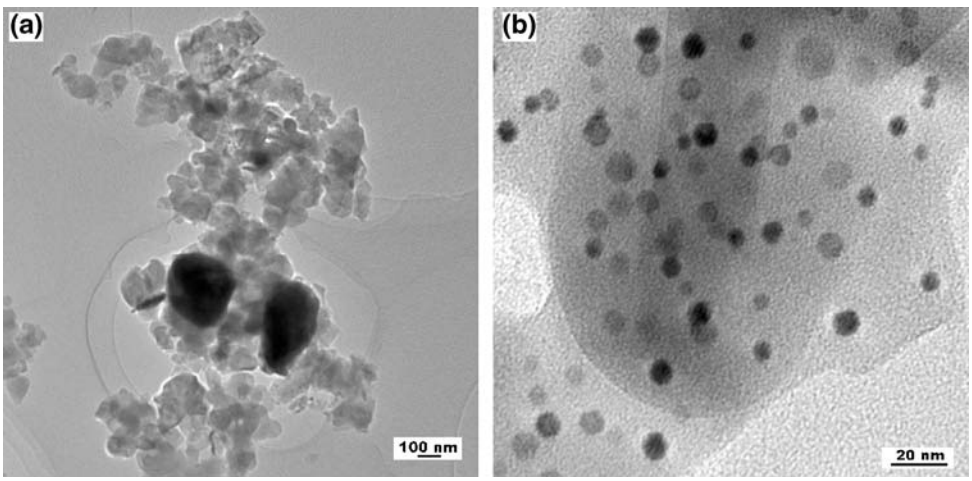

Fig. 2 The TEM images of reduced powders. ((**a**) Intergranular iron grains, (**b**) Intragranular iron nanoparticles embedded in mullite grain)

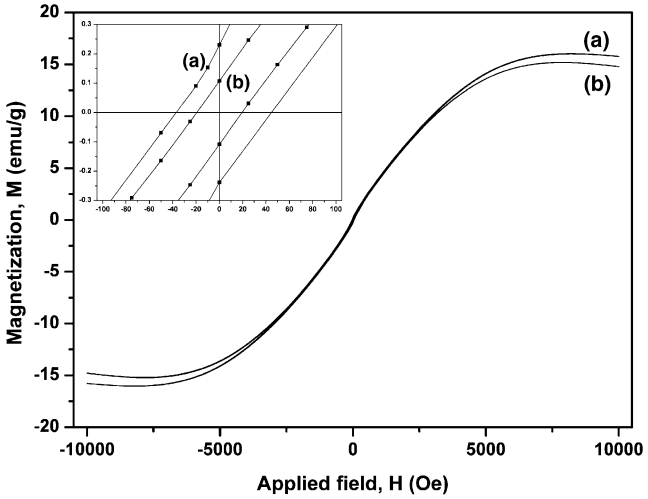

Fig. 3 The hysteresis loops for mullite–iron nanocomposite powders at different temperature. Insert shows enlargement of the plot near the origin. ((**a**) at 10 K, (**b**) at 300 K)

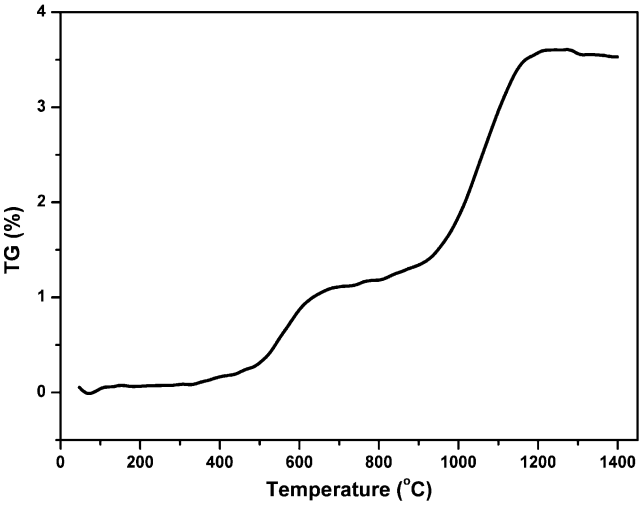

Fig. 5 The thermogravimetry curve of mullite–iron nanocomposite powders heated in air

embedded α-Fe nanoparticles in the mullite grains have a particle size less than 10 nm. Since metal cations in solid solution have different stability under reduction atmosphere, only Fe^{3+} can be reduced from the solid solution at 1,300 °C. The formation of intragranular nanoparticles is due to the precipitation of iron nanoparticles inside parent grains by changing the chemical state of iron cations through reduction. Mullite grain acts as a matrix to prevent the iron nanoparticles from further aggregation and growth.

Figure 3 shows the magnetic hysteresis loops for mullite–iron nanocomposite powders measured at temperature of 10 K (a) and 300 K (b). Saturated magnetizations (*Ms*), remanence ratio (*Mr/Ms*) and coercivity (*Hc*) of nanocomposite powders are 14.81 emu/g, 0.72%, 15 Oe at 300 K and 15.78 emu/g, 1.49%, 38 Oe at 10 K, respectively. It is known that for a superparamagnetic particle system, both the coercive field and remnant magnetization increase with decreasing temperature below the superparamagnetic-ferromagnetic transition temperature. And this increase is due to the lower thermal activation energy of spins at lower temperature. In our results, the variation of coercivity and remanence ratio with temperature implies the existence of superparamagnetic iron nanoparticles in mullite–iron nanocomposite powders. In magnetism, the temperature dependence of the magnetization for nano-sized magnetic particles reveals typical characteristics of superparamagnetism, showing the blocking temperature (T_B) at which the zero-field-cooled magnetization curve exhibits a cusp [14]. Figure 4 shows the result of magnetization versus temperature for field-cooled and zero-field-cooled experiments. It is found that a maximum appears at around 100 K in the zero-field-cooled curve, which is the blocking temperature. However, the zero-field-cooled and field-cooled magnetization curves do not completely overlap with each other above 100 K, which indicates the existence of ferromagnetic particles. As known, the magnetic behavior of metal nanoparticles is tightly related with their particle size. In the case of iron nanoparticles, the critical size of superparamagnetism is 14 nm [15]. From the observation of TEM, most of the intragranular iron nanoparticles are less than the critical size, which show the superparamagnetic behavior at room temperature. On the other hand, intergranular iron grains, with the size of hundreds of nanometers, are in the state of ferromagnetism at temperature above T_B.

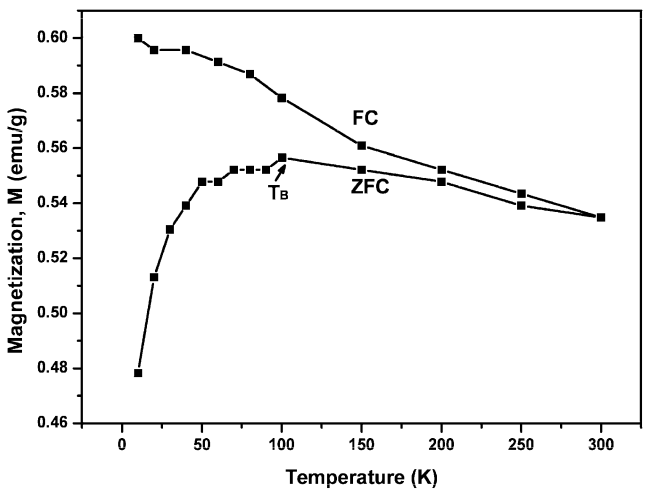

Fig. 4 The field-cooled and zero-field-cooled curves of mullite–iron nanocomposite powders reduced at 1,300 °C

The oxidation behavior of the mullite–iron nanocomposite powders was studied by heating them in air up to 1,400 °C. The thermogravimetry curve (Fig. 5) shows two stages of weight increment around 450 and 1,000 °C, respectively. The total mass gain of powders during the oxidation run is about 3.4%, which corresponds to the full transition of α-Fe (nominally, 7.81 wt% in reduced nano-

composite powders) to Fe^{3+} cation in $Al_{5.4}Fe_{0.6}Si_2O_{13}$. Since the intergranular iron grains are directly exposed to air, they have the similar oxidation temperature with pure iron powder (around 400 °C). On the contrary, it needs much higher temperature to penetrate the protection of mullite grain to oxidize the intragranular iron nanoparticles by oxygen. It is inferred that the lower oxidation temperature corresponds to the oxidation of intergranular iron grains and the higher one attributes to the oxidation of the iron nanoparticles embedded in mullite grains. Moreover, after comparing the amount of weight increment in two stages, it can roughly be estimated that about 64% of the total α-Fe phase in nanocomposite powders is dispersed as intragranular particles.

4 Conclusions

The mullite–iron composite powders have been successfully synthesized through the reduction of sol–gel prepared mullite–iron oxide solid solution at 1,300 °C. Two types of iron nanoparticles, the intergranular grains with the size around hundreds of nanometers and intragranular nanoparticles embedded in the grains of mullite, are formed in mullite–iron nanocomposite powders. The magnetic properties of nanocomposite powders suggest that the intergranular and intragranular α-iron nanoparticles have the ferromagnetic and superparamagnetic behavior at room temperature, respectively. The blocking temperature of intragranular α-iron nanoparticles is about 100 K. The oxidation behavior of nanocomposite powders shows that there exist two different oxidation stages of α-Fe nanoparticles. The intragranular α-iron nanoparticles have higher oxidation resistance than intergranular ones.

Acknowledgements This work was financially supported by the Natural Science Foundation of China (Contract No.50102003).

References

1. S. Sun, S. Andres, H.F. Hamann, J.-U. Tiele, J.E.E. Baglin, T. Thomson, E.E. Fullerton, C.B. Murray, B.D. Terris, J. Am. Chem. Soc. **124**, 2884 (2002)
2. J. Chatterjee, Y. Haik, C.-J. Chen, J. Magn. Magn. Mater. **246**, 382 (2003)
3. M. Matsumoto, Y. Miyata, J. Appl. Phys. **91**, 9635 (2002)
4. S.H. Sun, C.B. Murray, D. Weller, L. Folks, A. Moser, Science **287**, 1989 (2000)
5. K.S. Suslick, M. Fang, T. Hyeon, J. Am. Chem. Soc. **118**, 11960 (1996)
6. D.E. Weisshaar, T. Kuwana, J. Electroanal. Chem. **163**, 395 (1984)
7. H. Perez, J.P. Pradeau, P.A. Albouy, J. Perez-Omil, Chem. Mater. **11**, 3460 (1999)
8. V. Carles, Ch. Laurent, M. Brieu, A. Rousset, J. Mater. Chem. **9**, 1003 (1999)
9. I.A. Aksay, D.M. Dabbs, M. Sarikaya, J. Am. Ceram. Soc. **74**, 2343 (1991)
10. J. Parmentier, S. Vilminot, J. Alloys Compd. **264**, 136 (1998)
11. S.P. Chaudhuri, S.K. Patra, J. Mater. Sci. Lett. **35**, 4735 (2000)
12. H. Wang, T. Sekino, K. Niihara, Chem. Lett. **34**, 298 (2005)
13. P. Tartaj, T. González-Carreño, O. Bomatí-Miguel, C.J. Serna, Phys. Rev., B **69**, 094401 (2004)
14. M. Yoon, Y.M. Kim, Y. Kim, V. Volkov, H.J. Song, I.W. Park, J. Magn. Magn. Mater. **265**, 357 (2003)
15. J.F. Löffler, J.P. Meier, B. Doudin, J. Ansermet, W. Wagner, Phys. Rev., B **57**, 2915 (1998)